

Article

# A Comparative Study of Theoretical Methods to Estimate Semiconductor Nanoparticles' Size

Fernando Rodríguez-Mas <sup>\*</sup>, Juan Carlos Ferrer, José Luis Alonso, David Valiente  and Susana Fernández de Ávila

Communications Engineering Department, Universidad Miguel Hernández, 03202 Elche, Spain; j.c.ferrer@umh.es (J.C.F.); j.l.alonso@umh.es (J.L.A.); dvaliente@umh.es (D.V.); s.fdezavila@umh.es (S.F.d.Á.)

<sup>\*</sup> Correspondence: fernando.rodriguez@umh.es

Received: 25 February 2020; Accepted: 20 March 2020; Published: 21 March 2020



**Abstract:** In this paper, we compare four different methods to estimate nanoparticle diameters from optical absorption measurements, using transmission electron microscopy (TEM) images as a reference for the nanoparticle size. Three solutions of colloidal nanoparticles coated with thiophenol with different diameters were synthesized by thiolate decomposition. The nanoparticle sizes were controlled by the addition of a certain volume of a 1% sulphur solution in toluene. TEM measurements showed that the average diameter for each type of these nanoparticles was 2.8 nm, 3.2 nm, and 4.0 nm. The methods studied for the calculation of the nanoparticles diameter were: The Brus model, the hyperbolic band model (HBM), the Henglein model, and the Yu equation. We evaluated the importance of a good knowledge of the nanoparticle bandgap energy, and the nature of electronic transitions in the semiconductor. We studied the effects that small variations in the electron and hole effective mass values produced in the Brus equation and in the HBM model for CdS, PbS, and ZnS nanoparticles. Finally, a comparison was performed between the data provided by these models and the experimental results obtained with TEM images. In conclusion, we observed that the best approximation to the experimental results with TEM images was the Brus equation. However, when the bandgap energy was close to the bulk bandgap energy, the theoretical models did not adjust correctly to the size measured from the TEM images.

**Keywords:** cadmium sulphide nanoparticle; Brus model; hyperbolic band model; HBM; size estimation; TEM images

## 1. Introduction

Semiconductor nanoparticles (NPs), also known as quantum dots (QDs), have received great attention from the scientific community during the last few decades due to their potential applications. Far from decreasing, the interest has been growing over time because of the profusion of areas in which these structures may be useful, from optoelectronic devices [1–3] to biomedical applications [4].

Most of the methods found in the literature [5–8], which describe chemical routes to obtain nanoparticles in colloidal suspension, are based on the reaction of precursors in a solvent in the presence of stabilizing agents. These agents are usually represented by an organic radical, which is finally bonded to the QD surface [9]. The roles of these surface ligands are: (1) To stabilize the nanoparticles in order to prevent them from growing by material exchange (Ostwald ripening) [10], (2) to obtain solutions in the convenient solvents, and (3) to control the charge transfer between the particles and the surrounding material. Besides, the amount of stabilizer during the reaction of precursors is a key variable in the control of the nanoparticles' final size.

Since the physical properties of the semiconductor nanoparticles, like the bandgap, depend on their size due to quantum confinement of charge carriers, the availability of a method to assess

this magnitude becomes essential. Among the available methods to assess the size of nanoparticles, transmission electron microscopy (TEM) provides accurate measurements of the shape and size of structures in the scale of nanometers. Nonetheless, despite the good accuracy, this technique is far from being the most adequate for the quick measurement in routinely made multiple sets of samples. Alternative methods based on the data obtained in optical absorption measurements have been developed to estimate the nanoparticles' size. These methods are based on the determination of the edge of the absorption band, which, in turn, depends on the diameter of the nanocrystal.

The objective of this paper is the comparison of different methods based on both theoretical and empirical methods to be applied to the determination of the size of semiconductor nanoparticles. Several samples of CdS nanocrystals in colloidal suspension were synthesized by thiolate decomposition assisted by the addition of sulphur. The precise determination of the diameter was achieved by direct measurement from images obtained by TEM. Additionally, optical absorption spectra of the same samples were recorded. The absorption edge was calculated by means of the Tauc [11,12] relation. Subsequently, the size of the quantum dots was estimated using four well-known models: Brus model [13], hyperbolic band model (HBM) [14], Henglein formula [15], and the formula suggested by Yu et al. [16]. Finally, the influence of uncertainty of material parameters, such as the effective masses on the accuracy of the calculations, was studied.

## 2. Materials and Methods

### 2.1. Materials

Cadmium nitrate-tetrahydrate ( $\text{Cd}(\text{NO}_3)_2 \cdot 4\text{H}_2\text{O}$ , 99.99%), thiophenol ( $\text{C}_6\text{H}_5\text{-SH}$ ) (99%), sulphur powder (99.98%), toluene, methanol and dimethyl sulfoxide (DMSO) were purchased from Sigma-Aldrich (Darmstadt, Germany) and used without further purification.

### 2.2. Characterization

Optical absorption measurements were carried out with a T92+ UV-VIS spectrophotometer from PG Instruments Ltd. (Lutterworth, UK) and the measurements of photoluminescence (PL) performed with a Modular Spectrofluorometer Fluorolog-3 from Horiba Scientific (Madrid, Spain). In all photoluminescence measurements, the excitation wavelength was fixed at  $\lambda_{\text{exc}} = 365$  nm.

Transmission electron microscopy (TEM) analysis was taken by a Jeol 2010 (Tokyo, Japan) microscope operating at 200 kV. To carry out TEM measurements, a drop for each nanoparticle's solution was deposited on a carbon grid and then dried at room temperature. In order to obtain an accurate measurement of the nanoparticle sizes, TEM was calibrated by means of the measurement of the interplanar distance of standard gold nanoparticles.

In TEM microscopy, the factors that significantly limit resolution are: Spherical aberration, chromatic aberration, and astigmatism, with spherical aberration being the most critical. These aberrations and their implications are well known and a detailed study is beyond the scope of this paper. However, a thorough description may be found in any text about TEM technique [17]. The commented aberrations limit the resolution of our TEM device to 0.19 nm. This resolution is smaller than the space of (200) family planes used as a references for the nanoparticles' measurements [18].

### 2.3. Models

The following models relate the gap energy or the absorption edge with the size of the nanoparticles. Moreover, as the bandgap energy of the semiconductor was derived from the absorption edge, all models were based on the measurement of the nanoparticles' optical absorption. However, the determination of a value for this variable from the optical spectrum may become imprecise when the

excitonic peak is not clear. In these cases, the Tauc relation [11,12] provided a method to estimate the energy of the bandgap. The Tauc relation is defined as follows:

$$\alpha h\nu = A (h\nu - E_g)^n, \quad (1)$$

where  $E_g$  is the bandgap energy,  $n$  depends on the nature of the interband electronic transition, and  $A$  is an absorption constant [12]. Depending on the nature of the transition of the semiconductor,  $n$  can have the following values: For direct allowed transitions,  $n = 1/2$ ; for direct forbidden transitions,  $n = 3/2$ ; for indirect allowed transitions,  $n = 2$ ; and for indirect forbidden transitions,  $n = 3$ . For this relation, Tauc proposed an extrapolation to locate the absorption edge in semiconductors. For this reason,  $(\alpha h\nu)^{1/n}$  versus  $h\nu$  is plotted. By adjusting the variable  $n$  correctly, the absorption edge can be displayed.

### 2.3.1. Brus Model

Energy levels of the nanoparticles were discrete due to the quantum confinement of the charge carriers in the crystal. Brus et al. calculated the relation between the size and the electronic structure of the clusters. They related the effects of the quantum confinement to the nanoparticles radius and, consequently, postulated the following equation [13,19]:

$$E_n = E_b + (\hbar^2 \pi^2 / 2R^2) \times (1/m_e^* + 1/m_h^*) - 1.8e^2 / (4\pi\epsilon_0\epsilon R). \quad (2)$$

This formula expresses the relation between the energy gap of the nanoparticle,  $E_n$ , and the nanoparticle radius,  $R$ . The constants associated with the material are:  $E_b$ , the energy gap of bulk material;  $m_e^*$  and  $m_h^*$ , the effective masses of electrons and holes, respectively; and  $\epsilon$ , the dielectric constant.

Regarding the values of the effective masses of electrons and holes, these parameters are well known for bulk materials. However, when the quantum dots are small enough, the wavefunction overlaps with the crystal boundaries, and so the effective mass becomes energy dependent [20,21].

This could justify the different values of the electron and the hole effective masses for CdS nanoparticles that we have found in bibliography [22–24]. In addition, Henglein et al. comment on the difficulty of knowing the effective mass, since it can only be correctly known in electronic states close to the bandgap [25]. Therefore, a knowledge of the precise values of  $m_e^*$  and  $m_h^*$  is necessary to apply the Brus method. In this paper we will examine the possible effects that uncertainty of  $m_e^*$  and  $m_h^*$  could originate in the calculation of the size of some semiconducting monochalcogenides nanoparticles.

### 2.3.2. Hyperbolic Band Model (HBM)

Another method that relates bandgap and radius is the hyperbolic band model (HBM) [14]. In this model, a simple approximation is performed. Wang et al. indicate that the size-dependent Coulomb interaction of the Schrödinger equation for the crystallite excited state does not contribute significantly to small nanoparticles [26]. In consequence, they developed the HBM model, where the effective mass ( $m^*$ ) is defined by electrons' mass inside the semiconductor and free mass ( $m_0$ ) outside the semiconductor [27].

$$E_n^2 = E_b^2 + 2\hbar^2 \times E_b \times (\pi/R)^2 / m^*, \quad (3)$$

as in Brus equation,  $E_n$  and  $E_b$  are energy bandgap of nanoparticles and bulk semiconductor, respectively.

### 2.3.3. Empirical Formula Suggested by Henglein et al.

The previous Equations (2) and (3) describe methods which relate the gap energy with the cluster radius. Henglein synthesized several batches of CdS quantum dots by changing the pH. This resulted in nanoparticles with different sizes. Secondly, the authors measured the absorption edge of the

synthesized nanoparticles [28]. With this data, Moffitt et al. proposed an expression which relates the absorption wavelength ( $\lambda_a$ ) to the nanoparticles diameter ( $D$ ) [15],

$$D = 0.1 / (0.1338 - 0.0002345 \lambda_a). \quad (4)$$

#### 2.3.4. Empirical Formula Obtained by Yu et al.

Yu et al. have developed an empirical formula [16] that relates nanoparticles' diameter to wavelength of absorption edge ( $\lambda_a$ ). For the calculation of the expression, CdS NPs were synthesized by their research group where nanocrystals sizes were determined by transmission electron microscopy (TEM) measurements.

Then, graphs of the diameter versus wavelength of absorption edge were plotted. Thus, an empirical formula was achieved,

$$D = (-6.6521 \cdot 10^{-8}) \lambda_a^3 + (1.9557 \cdot 10^{-4}) \lambda_a^2 + (-9.2352 \cdot 10^{-2}) \lambda_a + 13.29. \quad (5)$$

#### 2.4. Synthesis of CdS Nanocrystals

The CdS nanoparticles were prepared at room temperature by thiolate decomposition [9]. In this method, the nanoparticle preparation route was divided into two stages: (1) The synthesis of a precursor material (cadmium thiolate) that contains both the metal and the organic radicals and (2) the decomposition of the thiolate by addition of sulphur resulting in the formation of CdS nanoparticles. To synthesize the cadmium thiolate, two solutions were prepared: 0.1 M of  $\text{Cd}(\text{NO}_3)_2 \cdot 4\text{H}_2\text{O}$  was dissolved in distilled water and methanol, with ratio 1:1, and 0.2 M  $\text{C}_6\text{H}_5\text{-SH}$  was dissolved in methanol. Both solutions were agitated in different flasks until they became homogeneous. When solutes of both solutions were completely dissolved, solutions were mixed together and stirred during 15 min. The blend evolved and turned a whitish color. Once filtered and dried, the cadmium thiolate ( $\text{Cd}(\text{C}_6\text{H}_5\text{S})_2$ ) was synthesized.

To provide the necessary sulphur for CdS NPs synthesis, stock sulphur solution with a concentration of 1% in toluene was prepared, from now on called  $V_{\text{(S(1\%)}}$ . Three different nanoparticle solutions were prepared. In three different vials,  $\text{Cd}(\text{C}_6\text{H}_5\text{S})_2$  was dissolved in DMSO by keeping the relation,  $m_{\text{(Cd(C}_6\text{H}_5\text{-SH))}}/V_{\text{(DMSO)}} = 40 \text{ mg/mL}$ , as shown in Table 1. These solutions were agitated and, when cadmium thiolate was dissolved, different volumes of  $V_{\text{(S(1\%)}}$  were added to each one. In the first one, 2.5 mL of  $V_{\text{(S(1\%)}}$  for each gram of  $\text{Cd}(\text{C}_6\text{H}_5\text{-SH)}$  were added. The mixture was stirred during 15 min and it became transparent and homogeneous. The output was the synthesis of CdS NPs with the following relation  $V_{\text{(S(1\%)}}/m_{\text{(Cd(C}_6\text{H}_5\text{-SH))}} = 2.5 \text{ mL/g}$ . For the synthesis of the other nanoparticles, two solutions with a relation  $V_{\text{(S(1\%)}}/m_{\text{(Cd(C}_6\text{H}_5\text{-SH))}} = 5.0$  and  $7.5 \text{ mL/g}$ , respectively, were selected. These nanoparticles are referenced as CdS(2.5), CdS(5.0), and CdS(7.5), respectively.

**Table 1.** Summary of the quantities used in the synthesis process of the CdS nanoparticles.

NPs	$m_{\text{[Cd(C}_6\text{H}_5\text{-SH)}}$	$V_{\text{[DMSO]}}$	$V_{\text{[S(1\%)}}$
CdS(2.5)	0.80 g	20 mL	2 mL
CdS(5.0)	0.80 g	20 mL	4 mL
CdS(7.5)	0.80 g	20 mL	6 mL

### 3. Results

#### 3.1. Optical Characterization

The absorbance and photoluminescence measurements were performed to the three types of nanoparticles. According to these measurements, their spectra are shown in Figure 1. The CdS(2.5) solution is plotted in black, the CdS(5.0) in red, and CdS(7.5) with blue lines. Figure 1A shows

normalized photoluminescence spectra for each CdS nanoparticle solution with dashed lines, with the absorbance spectra from the same solutions represented with solid lines.

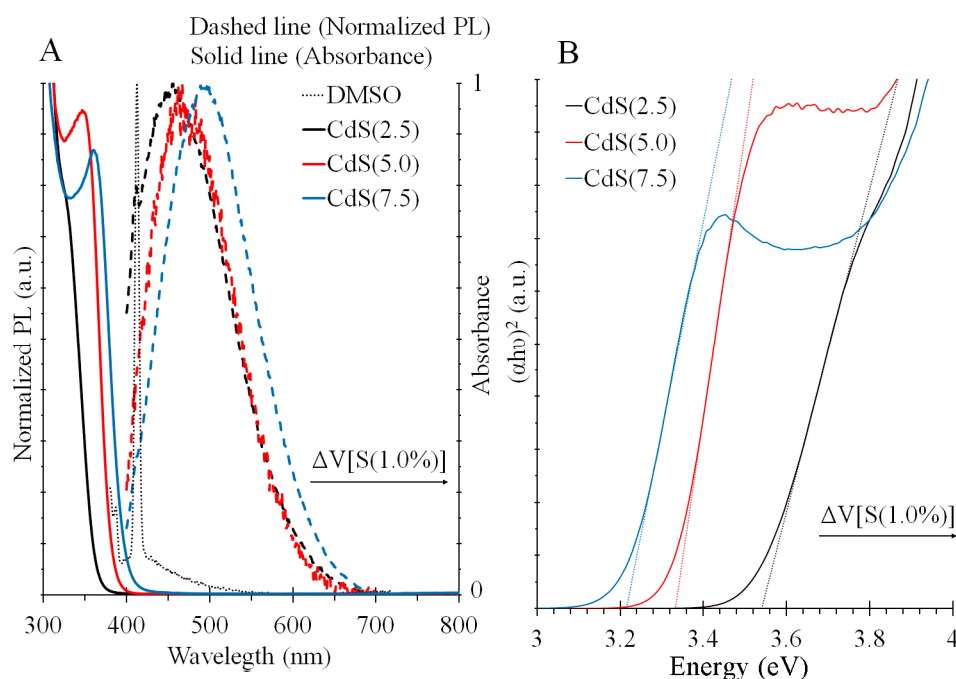


**Figure 1.** Normalized photoluminescence spectra, pristine optical absorption spectra (A) and optical absorption edge calculated using Tauc relation (B) for CdS nanoparticles synthesized by different volumes of sulphur in toluene. The 2.5, 5.0, and 7.5 milliliters of sulphur solution per gram of cadmium thiolate were used for the synthesis of each nanoparticle, respectively.

A broad dominant peak represents all PL curves from the colloidal CdS NPs. An asymmetry of these band shapes can be observed in Figure 1A. This is due to a reabsorption effect originated by size dispersion of the nanoparticles. Bigger NPs reabsorb a portion of the PL emission corresponding to the smaller nanocrystals, thus a slight red-shift of the wavelength of maximum emission was expected. This red-shift had no influence on the results presented in this work as they were mostly based on determination of the optical bandgap from the absorbance spectra.

The PL curve of CdS(2.5) exhibits a narrow peak at 413 nm lower than the dominant peak. This peak corresponds to DMSO solvent used in solutions. As Table 2 indicates, the wavelengths corresponding to the maximum emission from measured solutions were: 456 nm for CdS(2.5), 480 nm for CdS(5.0), and 495 nm for CdS(7.5). Increasing  $V_{(S(1\%))}$  in the synthesis led to higher wavelength in the PL emission of the nanocrystals.

**Table 2.** Absorption edge and photoluminescence peak of the CdS nanoparticles synthesized by 2.5, 5.0, and 7.5 milliliters of sulphur per gram of cadmium thiolate.

NPs	Absorption Edge		PL Peak
CdS(2.5)	3.54 eV	350 nm	456 nm
CdS(5.0)	3.33 eV	372 nm	480 nm
CdS(7.5)	3.21 eV	386 nm	495 nm

When we deal with monodisperse NPs, the presence of a clear excitonic peak allows an easier measurement of the energy gap. However, in the case of broad distribution, the excitonic peak is no longer clear and the use of the Tauc relation becomes necessary. The optical absorption spectra of the three samples are presented in Figure 1B. In this figure, the absorption edge moves to lower energies as

the addition of sulphur is increased. Accordingly, controlling sulphur volume in the synthesis route allowed us to synthesize nanoparticles with tailored sizes [29].

In Figure 2, photoluminescence and absorbance measurements were carried out for thiophenol and cadmium thiolate and compared with CdS NPs. Moreover, DMSO solvent spectra were included.

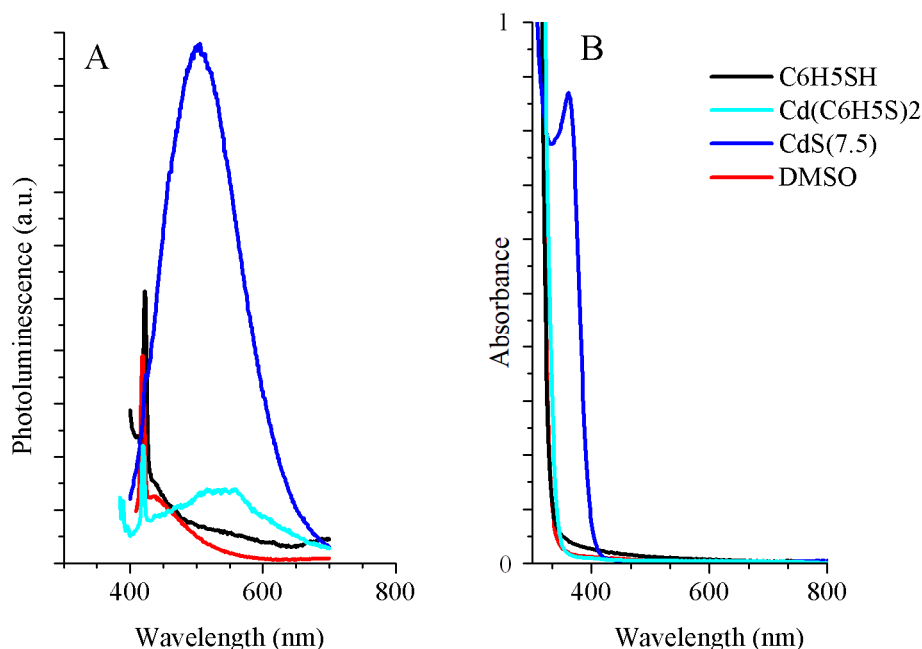


**Figure 2.** Photoluminescence spectra (A) and pristine optical absorption spectra (B) for thiophenol (black) and cadmium thiolate (cyan) CdS nanoparticles synthesized with 7.5 milliliters of sulphur solution per gram of cadmium thiolate in toluene (blue) and DMSO (red).

The measurements show that pristine thiophenol did not significantly influence photoluminescence and absorption measures. These spectra were very similar to DMSO solvent where they were dissolved for measurements. Although a slight contribution existed in photoluminescence regarding cadmium thiolate (cyan curve), its absorption was similar to thiophenol (black curve). Both absorption edges were located in the ultraviolet range. In contrast, its photoluminescence had a contribution around 500 nm. The difference in the chemical structure between thiophenol and cadmium thiolate was the presence of a S-Cd bond of thiolate inset of a presence of a S-H bond of thiophenol. Therefore, this commented contribution was attributable to the bond between ligand and cadmium. However, this contribution was very slight compared to the solvent.

### 3.2. TEM Study

TEM images corresponding to the previous three nanoparticle solutions are shown in Figure 3. It may be observed that some dispersion in nanoparticle size appears in the images. The size differences within each image corroborate the width of photoluminescence peak of CdS NPs observed in Figure 1A. Although the dispersion of size was present, we also observed that nanoparticles' sizes/diameters increased with the sulphur addition [30].

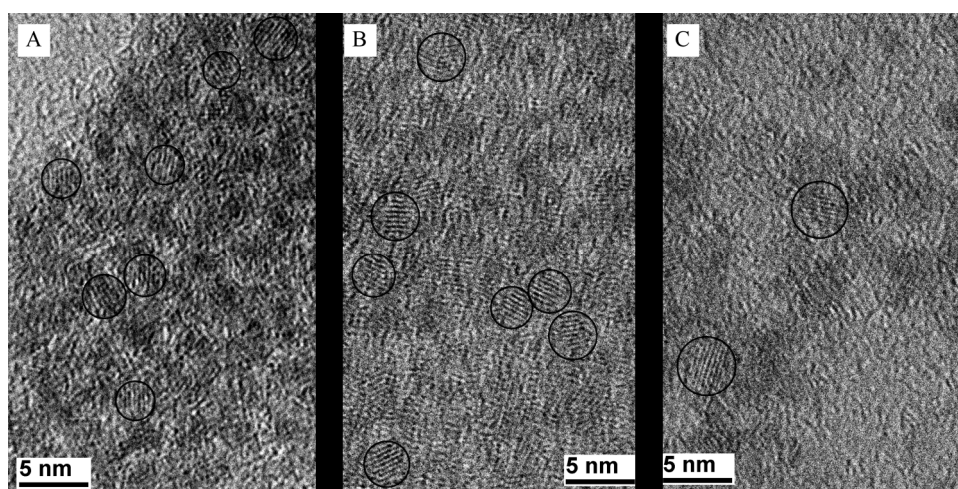


**Figure 3.** TEM images of CdS(2.5) (A), CdS(5.0) (B), and CdS(7.5) (C).

Regarding the size dispersion in TEM images, several nanoparticles were located for each sample. More than 150 nanoparticles for each sample were measured. Histograms were computed with localized nanoparticles, and represented in Figure 4. Figure 4A presents the histogram for CdS(2.5) in which the average size was 2.8 nm. Figure 4B shows the histogram for CdS(5.0), with average size of 3.2 nm. Finally, Figure 4C presents the histogram for CdS(7.5), which TEM average size was 4.0 nm. The size dispersion of the nanoparticles justified the full width at half maximum (FWHM) that was observed in the NPs' photoluminescence, Figure 1. Furthermore, FWHM, polydispersity, and the standard deviation were calculated for each size distribution. For CdS(2.5), FWHM was 1.53 nm, polydispersity was 27.36%, and standard deviation was 0.77 nm. For CdS(5.0), FWHM was 1.75 nm, polydispersity was 27.40%, and standard deviation was 0.88 nm. For CdS(7.5), FWHM was 1.87 nm, polydispersity was 23.43%, and standard deviation was 0.94 nm.

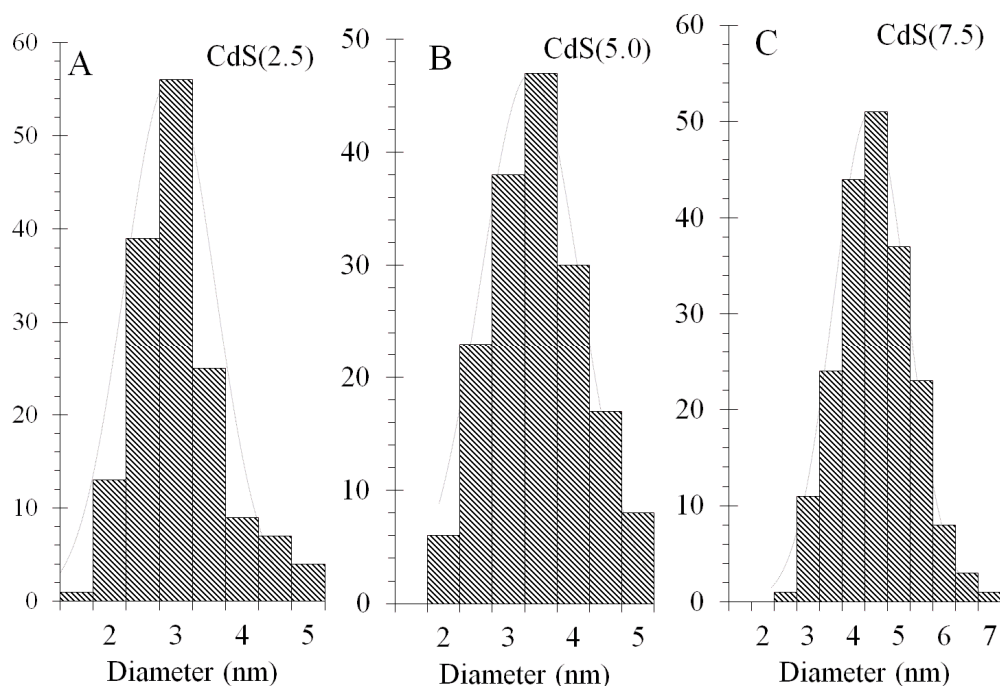


**Figure 4.** Histograms of different nanocrystals located in TEM analysis for each solution of CdS nanoparticles, for CdS(2.5) (A), for CdS(5.0) (B), and for CdS(7.5) (C).

### 3.3. Comparison of Theoretical Models to Estimate CdS Size

In this section, the sizes of the nanoparticles of the three samples were calculated by feeding four theoretical models with the data obtained from the optical spectra. The results obtained by the four models were compared to the experimental value obtained by direct measurement in TEM images. Additionally, we performed a study to assess the influence of the small variations on the effective mass of charge carrier on the calculated sizes.

As we commented in the introduction, the energy of the absorption edge was obtained using the method developed by Tauc et al. [11,12]. When applying the equation, the nature of the transition of the semiconductor, either direct or indirect, must be known. The energy of the absorption edge was obtained by extrapolating the linear interval of the low energy limit of the absorption band to the energy axis. In Figure 5A the bandgap energy for CdS(5.0) NPs was obtained from Tauc plot using different values of  $n$  to appreciate the differences. It was observed how increasing  $n$  value led to an overestimation of the size of the nanoparticle. Thus, knowing the nature of the electronic transitions in the semiconducting nanoparticle was a capital issue. For CdS NPs, the value  $n = 1/2$  was used since it is a direct bandgap material [31].

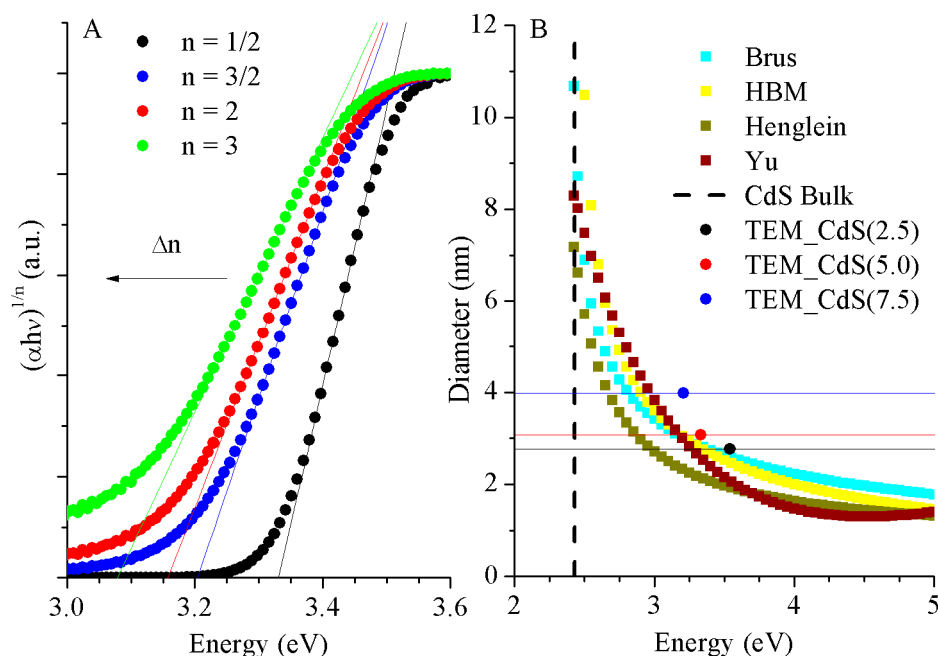


**Figure 5.** Graphs of Tauc relation with different  $n$  values for CdS nanoparticles (A), where  $n$  depends on the nature of interband electronic transition, varying between  $n = 1/2$ ,  $3/2$ ,  $2$ , and  $3$ . Different simulation (B) of nanoparticles' (NPs') sizes estimated with each model for CdS NPs as a function of bandgap energy. Horizontal lines set the average diameter of the nanoparticles calculated by the TEM images: CdS(2.5) (black line), CdS(5.0) (red line), and CdS(7.5) (blue line). The corresponding circle is located according to the optical gap calculated from absorbance spectra.

Once the bandgap energy was calculated, it was considered as the input parameter in each model. Figure 5B shows a comparison of the four models, with the material parameters corresponding to CdS. Additionally, three lines corresponding to the diameter of CdS NPs obtained by TEM images are shown, and circles are located at the bandgap energy obtained from Tauc equation for each nanoparticle. In this graph, we observe that for high bandgap energy all models produced a similar size. For example, for a 4.5 eV NP bandgap energy, the Brus equation estimated a diameter of 1.97 nm, for HBM of 1.68 nm, for the suggested Henglein equation the diameter would be 1.45 nm, and for the Yu empirical formula a 1.30-nm diameter. Dealing with diameter around 1.50 nm, the usual dispersion in size for colloidal nanocrystals was most probably in the range of the diameters estimated by these models.

Therefore, for higher energies of the absorption edge, all theoretical models studied in this work could be chosen as an alternative for calculating the CdS NPs' size because the difference between models can be admissible ( $\sim 0.6$  nm for 4.5 eV). On the other hand, for lower energies, the solutions given by the four models may show significant differences. For example, for 2.50 eV (getting close for the CdS bulk value, 2.42 eV [30]), the solutions of the theoretical models were 6.89 nm (Brus), 10.49 nm (HBM), 5.72 nm (Henglein), and 7.48 nm (Yu). The difference between the highest and the lowest value was 4.77 nm, which is a significant value compared to the obtained sizes. This is probably one of the reasons for the efforts dedicated by the scientific community to obtaining improved models.

Another remarkable observation from Figure 5B is related to CdS(7.5) NPs. The blue circle located using the bandgap energy measured from the Tauc relation did not match with any of the four models evaluated in this studies. All the models considered lower bandgaps for CdS NPs with 4.0 nm. This observation could also be extended to smaller nanoparticles, although for them it was not so striking.

Thinking about this mismatch, one issue to consider might be the role of the organic thiolated ligand on the optical properties of the nanoparticles, and its influence on the determination of the bandgap energy from the optical absorption spectra. It has been proved that ligands can influence the energy of NP electronic states changing the Coulomb interaction between the electron in the conduction band and the hole in the valence band inside a nanoparticle [32]. Bonding between ligands and inorganic core originates interfacial states with mixed NP–ligand character allowing core wavefunctions to extend across the inorganic/organic interface into the ligand shell, reducing the optical gap. This has been reported for CdSe and PbS NPs [29]. In our experiment, though, the indicated discrepancy could only be explained if the bonding between the CdS core and the thiol ligand was able to blue-shift the absorption edge of the nanocrystals. To our knowledge, this fact has not been referenced until now.

### 3.3.1. Brus Model

The first model used to estimate the size of the nanoparticles was the expression suggested by Brus. Diameters were calculated by solving Equation (2) for CdS(2.5), (5.0), and (7.5) samples. The calculated diameters were 2.59 nm, 2.83 nm, and 3.01 nm, respectively. For this estimation we employed the values of  $m_e^* = 0.19 \cdot m_0$  and  $m_h^* = 0.80 \cdot m_0$  used by Brus et al. in their studies [33]. However, small variations of the value of the effective masses may lead to significant differences on the calculated sizes. The effective masses of the electrons and the holes had different values depending on to the consulted bibliography. For example, on the one hand, Praus et al. indicated the values  $m_e^* = 0.18 \cdot m_0$  and  $m_h^* = 0.80 \cdot m_0$  [23]. In the other hand, Dey et al. reported  $m_e^* = 0.42 \cdot m_0$  and  $m_h^* = 0.61 \cdot m_0$  [24].

In Figure 6A, different diameter-energy gap curves are shown for several values of the hole effective mass. The  $m_h^*$  varied around the theoretical value,  $m_h^* = 0.80 \cdot m_0$ , whereas the other variables remained constant. The variations of the radius when the hole effective mass parameter was changed are more evident for values of the bandgap energy close to the bulk. For example, for  $E_g = 3.0$  eV, radiuses oscillated between 1.82 nm for  $m_h^* = 0.70 \cdot m_0$  to 1.62 nm for  $m_h^* = 0.90 \cdot m_0$ . In contrast to this, for an energy value of 2.44 eV, the difference in the radius reached 0.85 nm. The ranges were based on the most usual values that are found in the bibliography for the variables studied. The interval was selected adding a variation of  $0.1 \cdot m^*$  to the common value.

This comparison was also performed for the variable  $m_e^*$ . As in the previous study,  $m_e^*$  varied around the bulk value, in this case,  $m_e^* = 0.19 \cdot m_0$ . As detailed in Figure 6B, this variable was more critical than  $m_h^*$ . For  $E_g = 3.0$  eV, the radius varied between 1.88 and 1.64 nm for  $m_e^* = 0.10 \cdot m_0$  and  $m_e^* = 0.30 \cdot m_0$ , respectively. This difference increased for energies close to the bulk energy. It should also be noted that errors in  $m_e^*$  were more critical for energy gap close to CdS bulk. Small changes in  $m_e^*$  were determinant for energies close to the bulk energy (like in  $m_h^*$  variation study). Thus, accurate values for  $m_h^*$  and  $m_e^*$  should be used in order to avoid errors when using the Brus equation to estimate the size of quantum dots. Furthermore,  $m_e^*$  errors are more critical than  $m_h^*$  errors.

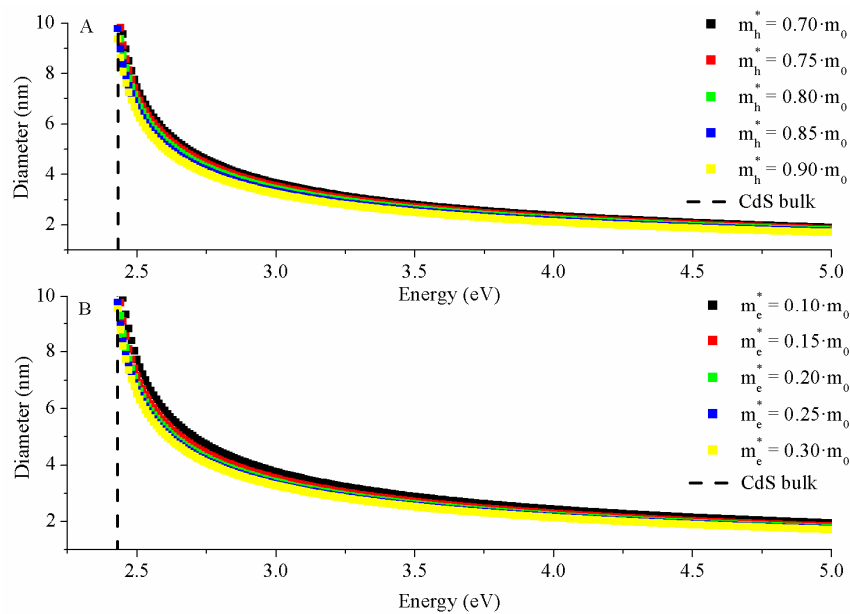


**Figure 6.** The  $m_h^*$  variation study (A) for Brus equation of CdS nanoparticles for different energies, from high values of energy to CdS energy bulk. The  $m_h^*$  oscillated between  $m_h^* = 0.70 \cdot m_0$  and  $m_h^* = 0.90 \cdot m_0$  with the rest of the variables remaining constant:  $E_b = 2.42$  eV,  $\epsilon = 5.7$ , and  $m_e^* = 0.19 \cdot m_0$ . The  $m_e^*$  simulation (B) for Brus equation of CdS nanoparticles for different energies, from high values of energy to CdS energy bulk. The  $m_e^*$  oscillated between  $m_e^* = 0.10 \cdot m_0$  and  $m_e^* = 0.30 \cdot m_0$  with the rest of the variables remaining constant:  $E_b = 2.42$  eV,  $\epsilon = 5.7$ , and  $m_h^* = 0.80 \cdot m_0$ .

These issues do not only arise in CdS NPs. They can also be observed in other semiconductor nanoparticles such as lead sulphide (PbS) or zinc sulphide (ZnS). The relation between the bandgap energy and nanoparticle diameter was been plotted for these two semiconductors. The following parameters were used: For PbS,  $E_g = 0.41$  eV,  $m_e^*$  from  $0.01 \cdot m_e^*$  to  $0.20 \cdot m_e^*$ ,  $m_h^*$  from  $0.01 \cdot m_h^*$  to  $0.20 \cdot m_h^*$ , and  $\epsilon = 17.2$  [34] and for ZnS,  $E_g = 3.70$  eV,  $m_e^*$  from  $0.30 \cdot m_e^*$  to  $0.50 \cdot m_e^*$ ,  $m_h^*$  from  $0.50 \cdot m_h^*$  to  $0.70 \cdot m_h^*$ , and  $\epsilon = 8.76$  [23].

In this sense, Figure 7 presents the obtained results for the PbS NPs estimated with the Brus equation. Figure 7B shows the study with  $m_e^*$  variation where the other Brus equation variables remained constant. For the  $E_n$  value kept constant, the increase in  $m_e^*$  value revealed a reduced PbS NPs diameter. It is noteworthy that for  $m_e^*$  values higher than  $m_e^* = 0.085 \cdot m_0$ , size variations were not critical. In Figure 7A, we can observe results for the  $m_h^*$  simulation. This study obtained the same results as  $m_e^*$  because the  $m_h^*$  and  $m_e^*$  were identical for PbS NPs.

In the case of ZnS nanoparticles, the study of the effect of  $m_h^*$  and  $m_e^*$  variation on the estimated size is shown in Figures 8A and 8B, respectively. Some results obtained were similar to results of CdS and PbS NPs tests. In Figure 8B, the  $m_e^*$  study showed that when  $m_e^*$  was increased nanoparticles' radius decreased. Additionally, for low bandgap energy values, close to bulk,  $m_e^*$  variations were more critical than at higher energy values. Concerning Figure 8A, to  $m_h^*$  its influence was less than  $m_e^*$ , although it followed the same trend. For instance, for energy values close to 3.7 eV, the ZnS energy bulk  $m_h^*$  variations became more important because small changes produced estimable differences in nanoparticles' size with respect to high energy values.

For both PbS NPs and ZnS NPs, results were similar to those obtained in the CdS NPs studies. Uncertainty in the  $m_e^*$  and  $m_h^*$  values produced size estimation errors, a fact that became critical when getting close to bulk energy gap values. To avoid calculation errors in the Brus equation, a correct data collection is necessary for the  $m_e^*$  and  $m_h^*$  values.

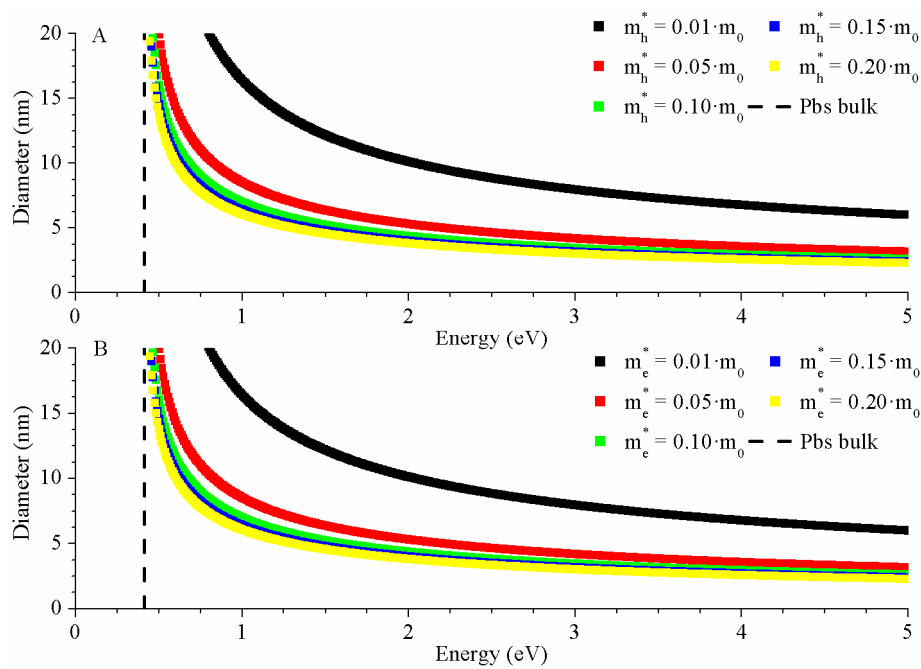


**Figure 7.** The  $m_h^*$  variation study (A) for Brus equation of PbS nanoparticles for different energies, from high values of energy to PbS energy bulk. The  $m_h^*$  oscillated between  $m_h^* = 0.01 \cdot m_0$  and  $m_h^* = 0.20 \cdot m_0$  with the rest of the variables remaining constant:  $E_b = 0.41$  eV,  $\epsilon = 17.2$ , and  $m_e^* = 0.085 \cdot m_0$ . The  $m_e^*$  simulation (B) for Brus equation of PbS nanoparticles for different energies, from high values of energy to PbS energy bulk. The  $m_e^*$  oscillated between  $m_e^* = 0.01 \cdot m_0$  and  $m_e^* = 0.20 \cdot m_0$  and with the rest of the variables remaining constant:  $E_b = 0.41$  eV,  $\epsilon = 17.2$ , and  $m_h^* = 0.085 \cdot m_0$ .

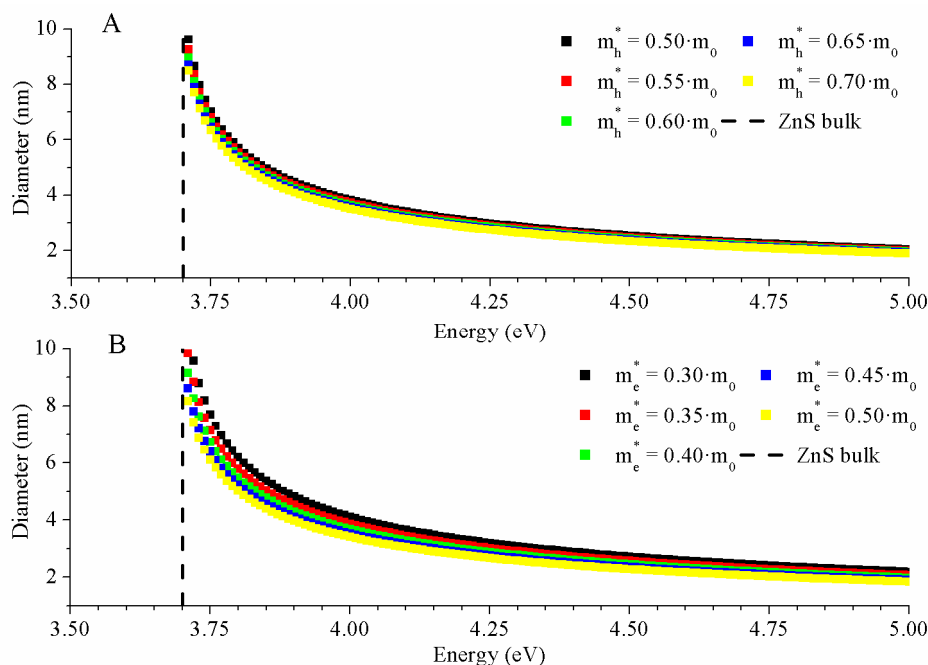


**Figure 8.** The  $m_h^*$  variation study (A) for Brus equation of ZnS nanoparticles for different energies, from high values of energy to ZnS energy bulk. The  $m_h^*$  oscillated between  $m_h^* = 0.50 \cdot m_0$  and  $m_h^* = 0.70 \cdot m_0$  and with the rest of the variables remaining constant:  $E_b = 3.70$  eV,  $\epsilon = 8.76$ , and  $m_e^* = 0.42 \cdot m_0$ . The  $m_e^*$  simulation (B) for Brus equation of ZnS nanoparticles for different energies, from high values of energy to ZnS energy bulk. The  $m_e^*$  oscillated between  $m_e^* = 0.30 \cdot m_0$  and  $m_e^* = 0.50 \cdot m_0$  and with the rest of the variables remaining constant:  $E_b = 3.70$  eV,  $\epsilon = 8.76$ , and  $m_h^* = 0.61 \cdot m_0$ .

### 3.3.2. HBM Model

In this section, the application of the hyperbolic band model (HBM) to the estimation of nanoparticle size is presented. As explained in Section 2.3.2, HBM employs the effective mass ( $m^*$ ) approximation. Solving the Equation (3) returned sizes of 2.47 nm, 2.79 nm, and 3.03 nm, respectively, for each synthesized nanoparticle (CdS(2.5), CdS(5.0), and CdS(7.5)).

In the Brus equation study, we observed that possible variations of  $m_e^*$  and  $m_h^*$  may modify the results obtained when estimating NPs' sizes. On the other hand, the HBM model simplified the effective masses of the electron and hole in a single mass, with the following equation:

$$1/m^* = 1/m_e^* + 1/m_h^*, \quad (6)$$

where  $m^*$  is the effective mass and  $m_e^*$  and  $m_h^*$  are the effective masses of electrons and holes, respectively. As in the Brus model,  $m_e^*$  and  $m_h^*$  variations were simulated and the effect on the HBM model was analysed.

The dependence of  $m^*$  with  $m_e^*$  and  $m_h^*$  (Equation (6)) makes the study of both variables necessary. In the test of the effective mass (Figure 9), it can be noted that when  $m_e^*$  or  $m_h^*$  increased,  $m^*$  increased. As in the previous studies, the NPs' size decreased when  $m^*$  increased. Additionally, for high bandgap energy values,  $m^*$  variations were not critical for both  $m_e^*$  and  $m_h^*$ . For example, for  $E_n = 4.5$  eV, the diameter varied between 1.92 nm and 1.73 nm for variations of  $m_h^*$  and it varied between 1.97 nm and 1.78 nm for variations of  $m_e^*$ . In energies close to energy CdS bulk, the  $m^*$  variations caused bigger differences in the size between extreme values (for  $E_n = 2.6$  eV, the difference is 0.75 nm for variations of  $m_h^*$ , and for variations of  $m_e^*$  the difference was 0.88 nm), but as the NP size was bigger, the relative error in the diameter estimation was negligible.

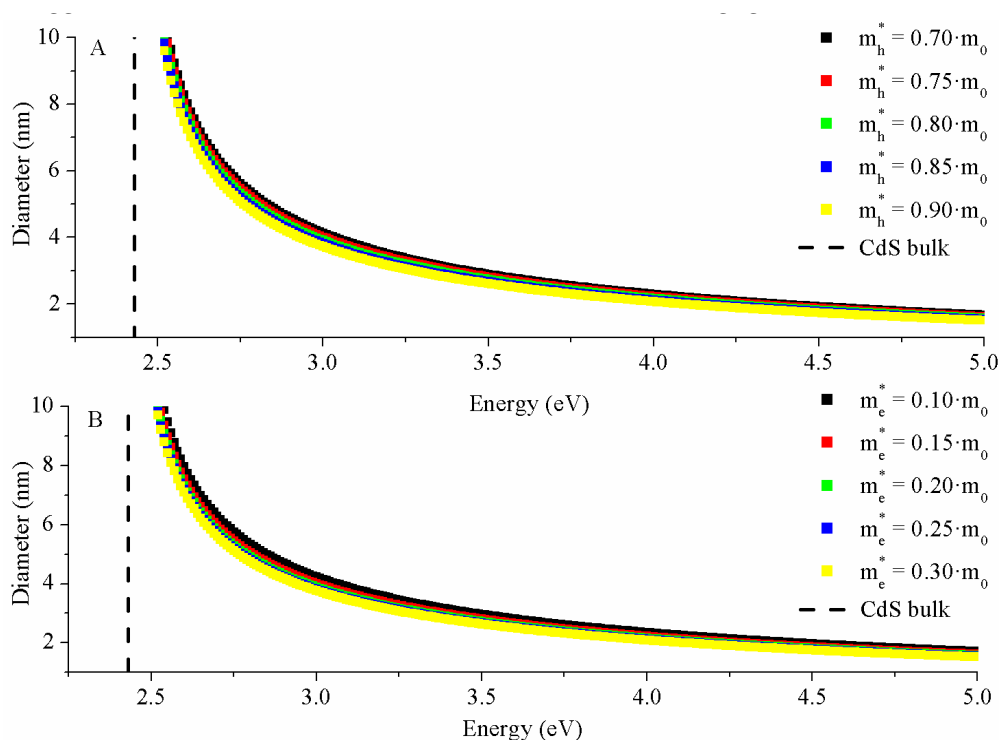


**Figure 9.** Estimated CdS NPs' size by the hyperbolic band model (HBM) model as a function of nanoparticle bandgap energy with (A)  $m_h^*$  and  $m_e^*$  (B) as parameters. The  $m_h^*$  oscillated between  $m_h^* = 0.70 \cdot m_0$  and  $m_h^* = 0.90 \cdot m_0$  and  $m_e^*$  oscillated between  $m_e^* = 0.10 \cdot m_0$  and  $m_e^* = 0.30 \cdot m_0$ , with  $E_b$  remaining constant,  $E_b = 2.42$  eV.

Subsequently, for the HBM model, we observed results for  $m_e^*$  and  $m_h^*$  variations for PbS (Figure 10) and for ZnS (Figure 11) NPs. For PbS and ZnS simulations, the results were similar to the CdS NPs' simulations. An increase of  $m_e^*$  and  $m_h^*$  augmented the effective mass. This fact modified HBM model results, where the diameters were smaller due to the growth of  $m^*$ . As in CdS, PbS, and ZnS NPs, variations towards low energies increased nanoparticles' dimensions.

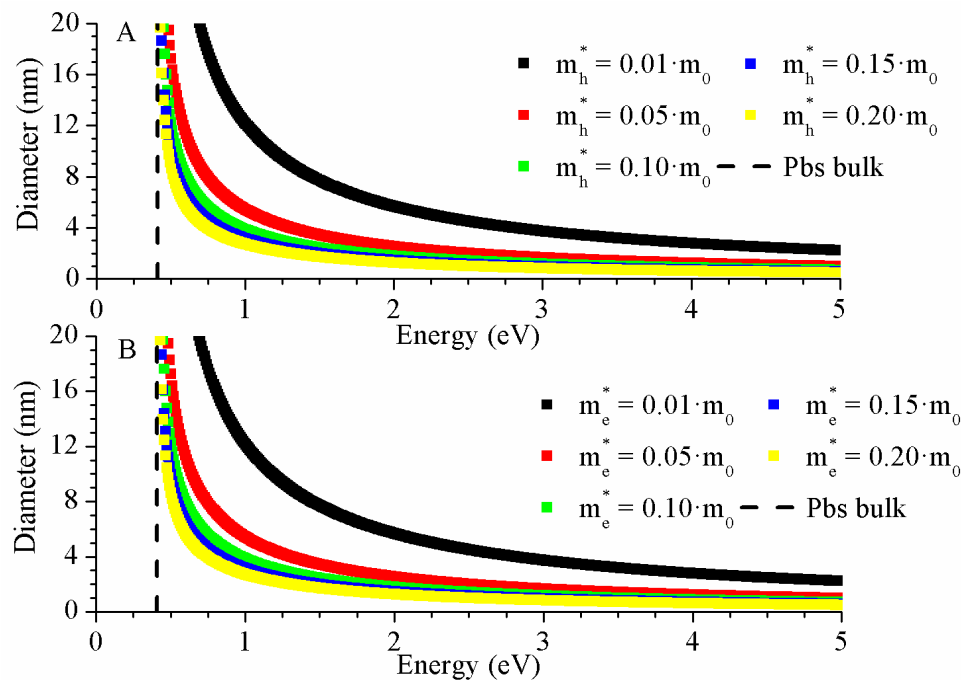


**Figure 10.** Estimated PbS NPs' size by HBM model as a function of nanoparticle bandgap energy with (A)  $m_h^*$  and  $m_e^*$  (B) as parameters. The  $m_h^*$  oscillated between  $m_h^* = 0.01 \cdot m_0$  and  $m_h^* = 0.20 \cdot m_0$  and  $m_e^*$  oscillated between  $m_e^* = 0.01 \cdot m_0$  and  $m_e^* = 0.20 \cdot m_0$ , with  $E_b$  remaining constant,  $E_b = 0.41$  eV.

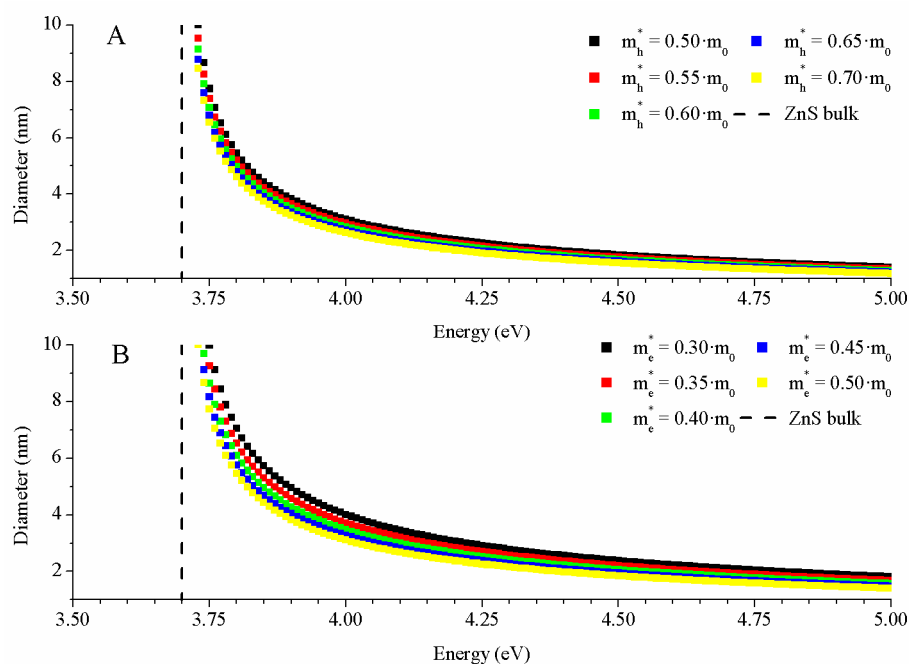


**Figure 11.** Estimated ZnS NPs' size by HBM model as a function of nanoparticle bandgap energy with (A)  $m_h^*$  and  $m_e^*$  (B) as parameters. The  $m_h^*$  oscillated between  $m_h^* = 0.50 \cdot m_0$  and  $m_h^* = 0.70 \cdot m_0$  and  $m_e^*$  oscillated between  $m_e^* = 0.30 \cdot m_0$  and  $m_e^* = 0.50 \cdot m_0$ , with  $E_b$  remaining constant,  $E_b = 3.70$  eV.

Modifications of  $m_h^*$ , the  $m_e^*$ , and  $m^*$  variables were critical when the energy gap was close to the bulk energy. Then, both the calculation of the absorption edge and an exact value of the effective mass became critical for a correct use of theoretical models to calculate the size of the nanoparticles. Attending to Figures 9 and 11 versus Figures 6 and 8, it is remarkable that HBM led to bigger nanoparticle diameter when energy was close to the bulk bandgap, contrasting with the Brus equation. This was observed for CdS and ZnS NPs, but not for PbS NPs. This result could be expected because the Brus model uses infinite square well-type quantum confinement.

### 3.3.3. Henglein Model and Yu Equation

Now, the empirical models that describe the direct relation between the absorption wavelength ( $\lambda_a$ ) and the diameter will be addressed.

The sizes of CdS NPs according to Henglein (Equation (4)) were 1.94 nm for CdS(2.5), 2.15 nm for CdS(5.0), and 2.31 nm for CdS(7.5), respectively.

The last formula to be considered arose from an empirical model developed by Yu et al. The sizes calculated from the Equation (5) were 2.08 nm, 2.58 nm, and 2.96 nm, respectively.

The summary of the results is presented in Figure 12 and Table 3.

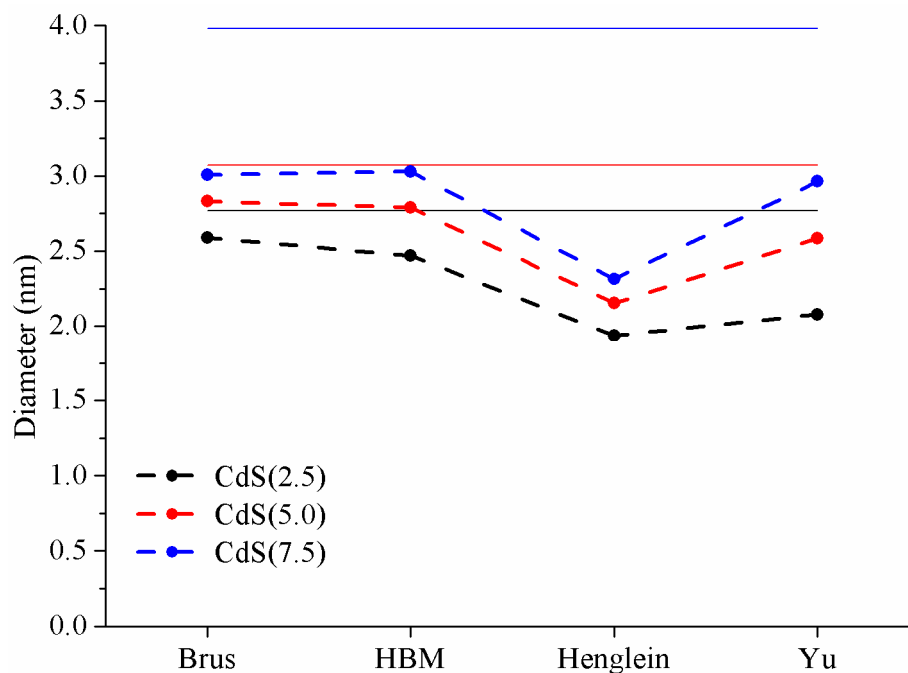


**Figure 12.** Comparison among the nanoparticles' size obtained with the theoretical methods studied in this paper and the experimental values obtained with TEM images (solid lines).

**Table 3.** Results' deviation between the different theoretical models estimation for the size and the real measurements obtained with TEM analysis.

NPs	Brus	HBM	Henglein	Yu
CdS(2.5)	−6%	−11%	−30%	−25%
CdS(5.0)	−8%	−9%	−30%	−16%
CdS(7.5)	−24%	−24%	−42%	−26%

Figure 12 shows that, in general, the numerical result obtained from the four models was lower than the mean size measured in the TEM images (negative sign in Table 3). Additionally, the models that were closest to the TEM image measurements were those that related the absorption edge energy to the nanoparticle radius. Both the Brus equation and HBM model showed similar results for the

three samples and were more accurate for smaller NP diameters. The empirical models presented less accurate size estimation than their theoretical counterparts, especially the Henglein model. A remarkable observation was that all models evidenced poorer results for larger nanoparticles. As we showed in Figure 5B, the dispersion of results was bigger when the absorption edge was slightly higher than bulk energy. In other words, models were more imprecise when nanoparticles were bigger. In these cases, it was crucial to know the accurate value for the bandgap energy of the NP.

The difference between the diameter estimated empirically by the TEM images and the theoretical result decreased for the smaller nanoparticles. These differences may be considered negligible, since they may be smaller than the dispersion of sizes present in as-synthesized colloidal NPs.

#### 4. Conclusions

CdS nanoparticles were synthesized by thiolate decomposition. The CdS size was controlled by the addition of sulphur in the synthesis process. It was verified that the size of the nanoparticles increased with the addition of sulphur.

Optical absorption and photoluminescence characterization of three different samples of nanoparticles were performed and their size was calculated using four theoretical methods: The Brus equation, the HBM formula, and the empirical formulas by Henglein et al. and Yu et al., respectively. TEM study was performed and we verified that for small sizes, the Brus model was the most accurate. The Brus and HBM models presented very similar results for CdS NPs, but for PbS and ZnS NPs the HBM always estimated smaller diameters compared to Brus for the same bandgap energy of the NPs. In addition, the HBM model was more sensitive to knowing the exact value of  $E_n$  due to sharp variation of size for energies closest to NPs'  $E_b$ , especially for PbS NPs. In our experiment with CdS NPs, the worse estimation of sizes was obtained by the Henglein formula.

Issues arising from imprecise material parameter knowledge were evaluated. In the theoretical models studied, it is noteworthy that masses did not affect the estimation of size significantly. To obtain an accurate value of the bandgap energy of the NP is more significant for size estimation than effective mass. However,  $m_e^*$ ,  $m_h^*$ , and  $m^*$  parameters must be well known, since errors in their values may lead to nonnegligible errors in the size estimation, especially for energies slightly higher than the bulk bandgap. These considerations must be taken into account in the theoretical models, regardless of the type of nanoparticles that are being studied.

**Author Contributions:** F.R.-M. designed the experiments; F.R.-M. performed the experiments; F.R.-M., J.C.F., J.L.A., and S.F.d.Á. analyzed the data; F.R.-M. wrote the original paper draft; J.C.F. and S.F.d.Á. supervised and performed critical revisions of the paper; S.F.d.Á., J.L.A., and D.V. revised the manuscript. All authors have read and agreed to the published version of the manuscript.

**Funding:** This research was supported financially by the Conselleria d'Educació, Investigació, Cultura i Esport from Generalitat Valenciana under the projects GV/2017/012 and AICO/2017/148.

**Conflicts of Interest:** The authors declare no conflict of interest.

#### References

1. Kiyohara, S.; Fujiwara, M.; Matsubayashi, F.; Mori, K. Organic light-emitting microdevices fabricated by nanoimprinting technology using diamond molds. *Jpn. J. Appl. Phys.* **2005**, *44*, 3686–3690. [[CrossRef](#)]
2. Pu, Y.; Chen, Y. Solution-processable bipolar hosts based on triphenylamine and oxadiazole derivatives: Synthesis and application in phosphorescent light-emitting diodes. *J. Lumin.* **2016**, *170*, 127–135. [[CrossRef](#)]
3. Alonso, J.L.; Ferrer, J.C.; Rodríguez-Mas, F.; Fernández de Ávila, S. Improved P3HT:PCBM photovoltaic cells with two-fold stabilized PbS nanoparticles. *Optoelectron. Adv. Mat.* **2016**, *10*, 634–639.
4. Pugazhendhi, A.; Edison, T.N.J.I.; Karuppusamy, I.; Kathivel, B. Inorganic nanoparticles: A potential cancer therapy for human welfare. *Int. J. Pharm.* **2018**, *539*, 104–111. [[CrossRef](#)]
5. Pavel, F.M.; Mackay, R.A. Reverse micellar synthesis of a nanoparticle/polymer composite. *Langmuir* **2000**, *16*, 8568–8574. [[CrossRef](#)]

6. Feldheim, D.L.; Keating, C.D. Self-assembly of single electron transistors and related devices. *Chem. Soc. Rev.* **1998**, *27*, 1–12. [[CrossRef](#)]
7. Granot, E.; Patolsky, F.; Willner, I. Electrochemical assembly of a CdS semiconductor nanoparticle monolayer on surfaces: Structural properties and photoelectrochemical applications. *J. Phys. Chem. B* **2004**, *108*, 5875–5881. [[CrossRef](#)]
8. Cordoncillo, E.; Escribano, P.; Monrós, G.; Tena, M.A.; Orera, V.M.; Carda, J. The preparation of CdS particles in silica glasses by a sol-gel method. *J. Solid State Chem.* **1995**, *118*, 1–5. [[CrossRef](#)]
9. Ferrer, J.C.; Salinas-Castillo, A.; Alonso, J.L.; Fernández de Ávila, S.; Mallavia, R. Direct synthesis of PbS nanocrystals capped with 4-fluorothiophenol in semiconducting polymer. *Mater. Chem. Phys.* **2010**, *122*, 459–462. [[CrossRef](#)]
10. Schmitt, S.; Arditty, S.; Leal-Calderon, F. Stability of concentrated emulsions. *Interface Sci. Technol.* **2004**, *4*, 607–639. [[CrossRef](#)]
11. Tauc, J.; Menth, A. State in the gap. *J. Non-Cryst. Solids* **1972**, *8–10*, 569–585. [[CrossRef](#)]
12. Osuwa, J.C.; Oriaku, C.I.; Kalu, I.A. Variation of optical band gap with post deposition annealing in CdS/PVA thin films. *Chalcogenide Lett.* **2009**, *6*, 433–436.
13. Brus, L. Electronic wave functions in semiconductor clusters: Experiment and theory. *J. Phys. Chem.* **1986**, *90*, 2555–2560. [[CrossRef](#)]
14. Das, R.; Pandey, S. Comparison of optical properties of bulk and nano crystalline thin films of CdS using different precursors. *Int. J. Mater. Sci.* **2011**, *1*, 35–40.
15. Moffitt, M.; Eisenber, A. Size Control of nanoparticles in Semiconductor-Polymer Composites. 1. Control via Multiplet Aggregation Numbers in Styrene-Based Random Ionomers. *Chem. Mater.* **1995**, *7*, 1178–1184. [[CrossRef](#)]
16. Yu, W.W.; Qu, L.H.; Guo, W.Z.; Peng, X.G. Experimental Determination of the Extinction Coefficient of CdTe, CdSe, and CdS Nanocrystals. *Chem. Mater.* **2003**, *15*, 2854–2860. [[CrossRef](#)]
17. Reimer, L.; Kohl, H. *Transmission Electron Microscopy. Physics of Image Formation*, 5th ed.; Elsevier: Heidelberg, Germany, 2008; ISBN 978-1-4419-2308-0.
18. Rodríguez-Mas, F.; Fernández de Ávila, S.; Ferrer, J.C.; Alonso, J.L. Expanded Electroluminescence in High Load CdS Nanocrystals PVK-Based LEDs. *Nanomaterials* **2019**, *9*, 1212. [[CrossRef](#)]
19. Hullavard, N.V.; Hullavard, S.S.; Karulkar, P.C. Cadmium sulphide (CdS) nanotechnology: Synthesis and applications. *J. Nanosci. Nanotechnol.* **2008**, *8*, 3272–3299. [[CrossRef](#)]
20. Zhou, A.P.; Sheng, W.D. Electron and hole effective masses in self-assembled quantum dots. *Eur. Phys. J. B.* **2009**, *68*, 233–236. [[CrossRef](#)]
21. Tan, S.G.; Jalil, M.B.A. 2—Nanoscale physics and electronics. In *Introduction to the Physics of Nanoelectronics*, 1st ed.; Woodhead Publishing Limited: Cambridge, UK, 2012; pp. 23–77. [[CrossRef](#)]
22. Unni, C.; Philip, D.; Smitha, S.L.; Nissamudeen, K.M.; Gopchandran, K.G. Aqueous synthesis and characterization of CdS, CdS:Zn<sup>2+</sup> and CdS:Cu<sup>2+</sup> quantum dots. *Spectrochim. Acta A Mol. Biomol. Spectrosc.* **2009**, *72*, 827–832. [[CrossRef](#)]
23. Praus, P.; Svoboda, L.; Horínková, P. Preparation and optical absorption of CdS, ZnS, ZnXCd1-XS and core/shell CdS/ZnS nanoparticles. *Nanocon* **2013**, *10*, 16–18.
24. Dey, P.C.; Das, R. Photoluminescence quenching in ligand free CdS nanocrystals due to silver doping along with two high energy surface states emission. *J. Lumin.* **2017**, *183*, 368–376. [[CrossRef](#)]
25. Henglein, A. Small-particle research: Physicochemical properties of extremely small colloidal metal and semiconductor particles. *Chem. Rev.* **1989**, *89*, 1861–1873. [[CrossRef](#)]
26. Wang, Y.; Suna, A.; Mahler, W.; Kasowski, R. PbS in polymers. From molecules to bulk solids. *J. Chem. Phys.* **1987**, *87*, 7315–7322. [[CrossRef](#)]
27. Nanda, K.K.; Kruis, F.E.; Fissan, H.; Behera, S.N. Effective mass approximation for two extreme semiconductors: Band Gap of PbS and CuBr nanoparticles. *J. Appl. Phys.* **2004**, *95*, 5035. [[CrossRef](#)]
28. Spanhel, L.; Haase, M.; Weller, H.; Henglein, A. Photochemistry of colloidal semiconductors. 20. Surface modification and stability of strong luminescing CdS particles. *J. Am. Chem. Soc.* **1987**, *109*, 5649–5655. [[CrossRef](#)]
29. Boles, M.A.; Ling, D.; Hyeon, T.; Talapin, D.V. The surface science of nanocrystals. *Nat. Mater.* **2016**, *15*, 141–153. [[CrossRef](#)]

30. Ferrer, J.C.; Salinas-Castillo, A.; Alonso, J.L.; Fernández de Ávila, S.; Mallavia, R. Influence of SPP co-stabilizer on the optical properties of CdS quantum dots grown in PVA. *Phys. Procedia* **2009**, *2*, 335–338. [[CrossRef](#)]
31. Heiba, Z.K.; Mohamed, M.B.; Imam, N.G. Fine-tune optical absorption and light emitting behavior of the CdS/PVA hybridized film nanocomposite. *J. Mol. Struct.* **2017**, *1136*, 321–329. [[CrossRef](#)]
32. Ning, Z.; Molnár, M.; Chen, Y.; Friberg, P.; Gan, L.; Ågren, H.; Fu, Y. Role of surface ligands in optical properties of colloidal CdSe/CdS quantum dots. *Phys. Chem. Chem. Phys.* **2011**, *13*, 5848–5854. [[CrossRef](#)]
33. Brus, L. Electron-electron and electron-hole interactions in small semiconductor crystallites: The size dependence of the lowest excited electronic state. *J. Chem. Phys.* **1984**, *80*, 4403–4409. [[CrossRef](#)]
34. Souci, A.H.; Keghouche, N.; Delaire, J.A.; Remita, H.; Etcheberry, A.; Mostafavi, M. Structural and Optical Properties of PbS Nanoparticles Synthesized by the Radiolytic Method. *J. Phys. Chem. C* **2009**, *113*, 8050–8057. [[CrossRef](#)]



© 2020 by the authors. Licensee MDPI, Basel, Switzerland. This article is an open access article distributed under the terms and conditions of the Creative Commons Attribution (CC BY) license (<http://creativecommons.org/licenses/by/4.0/>).